Development and Extension of An Aggregated Scale Model
Part 1 – Background to ASMITA

Townend, I; Wang, Zheng Bing; Stive, Marcel; Zhou, Z.

DOI
10.1007/s13344-016-0030-x

Publication date
2016

Document Version
Proof

Published in
China Ocean Engineering

Citation (APA)
Townend, I., Wang, Z. B., Stive, M., & Zhou, Z. (2016). Development and Extension of An Aggregated Scale Model: Part 1 – Background to ASMITA. *China Ocean Engineering*, *30*(4), 483-504. https://doi.org/10.1007/s13344-016-0030-x

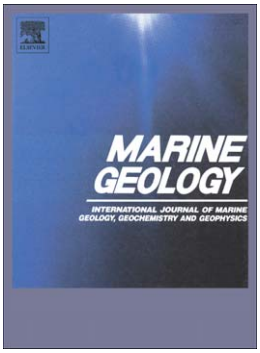

¡!–¡query id="q2" type="boolean" replies="Yes—No"¿¡ce:para¿Your article is registered as a regular item and is being processed for inclusion in a regular issue of the journal. If this is NOT correct and your article belongs to a Special Issue/Collection please contact s.ananthakrishnan@elsevier.com immediately prior to returning your corrections.¡/ce:para¿¡/query¿–¿Coupling bedform roughness and sediment grain-size sorting in modelling of tidal inlet incision

¡!–¡query id="q3" type="boolean" replies="Yes—No"¿¡ce:para¿The author names have been tagged as given names and surnames (surnames are highlighted in teal color). Please confirm if they have been identified correctly.¡/ce:para¿¡/query¿–¿Yunwei Wang, Qian Yu, Jian Jiao, Pieter Koen Tonnon, Zheng Bing Wang, Shu Gao

PII: S0025-3227(16)30190-6
DOI: doi: 10.1016/j.margeo.2016.09.004
Reference: MARGO 5506

To appear in: *Marine Geology*

Received date: 27 December 2015
Revised date: 3 September 2016
Accepted date: 6 September 2016

Coupling bedform roughness and sediment grain-size sorting in modelling of tidal inlet incision

Yunwei Wang[a, b, c], Qian Yu[d, c *], Jian Jiao[e, b, c], Pieter Koen Tonnon[b], Zheng Bing Wang[b, c], Shu Gao[f]

a College of Harbour, Coastal and Offshore Engineering, Hohai University, Nanjing, China.

[b] Deltares, Delft, The Netherlands

[c] Faculty of Civil Engineering and Geosciences, Delft University of Technology, Delft, The Netherlands

[d] MOE Key Laboratory for Coast and Island Development, Nanjing University, Nanjing, China ([*] qianyu.nju@gmail.com)

[e] Nanjing Hydraulic Research Institute, Nanjing, China

[f] State Key Laboratory for Estuarine and Coastal Studies, East China Normal University, Shanghai, China

Abstract:

A key problem in the decadal morphodynamic modelling of tidal inlet system is on the evolution of the inlet channels, especially the unrealistic channel incision. The present study attempts to couple two processes, including the bedform roughness and sediment grain-size sorting, in the two-dimensional, depth-averaged process-based model to solve the problem. Based on the comparison of the modelling results and relevant field observations in the Dutch Wadden Sea, it is suggested that bedform roughness height predictor is a useful tool for determining spatial and temporal heterogeneous bed frictions. Within tidal channels, bedform roughness is dominated by dune roughness. In order to represent "the memory of old bedforms", a relaxation time method was implemented. The corresponding large relaxation time (2 M2 tidal periods) smooths the tidal variations of dune roughness, and makes it respond to hydrodynamic changes on a longer time scale. When decadal morphological modelling is carried out, the model performance can be significantly improved by introducing either bedform (dune) roughness predictor or sediment sorting processes. The mechanisms are twofold. First, in the deep channels where flow velocities are high, large dunes develop and cause large bed drag coefficients. Second, coarser bed sediments within the channel area induced by sorting prevent the channel incision. If both effects are coupled in the morphodynamic modelling, the inlet channel incision is further controlled, which is not just a result of the linear superposition of both effects, because sorting can further promote the development of dunes within the deep channels.

Keywords: bedform roughness; grain-size sorting; inlet incision; Dutch Wadden Sea

1. Introduction

Tidal inlets and basins are important for economic, ecological and environmental reasons, e.g., by providing natural harbors, inland waterways, land resources, and marine invertebrates, fishes and birds (Reise, 2001; Anthony et al., 2009). To cope with the impacts of sea-level rise and human activities (e.g. land reclamation, harbor construction), a thorough understanding of the characteristics of tidal inlet morphodynamics is fundamentally necessary, so as to predict the morphological responses to these changes and to make appropriate decisions for management (Lee et al., 1999; van Goor et al., 2003; FitzGerald et al., 2008; van der Wegen, 2013).

Tidal inlets are complex dynamic systems, including a number of elements, e.g., inlet channels, flood-tidal deltas, ebb-tidal deltas, the adjacent beaches, dunes on barrier islands, and back-barrier tidal basins (de Swart and Zimmerman, 2009). Influenced by the external forces of tides, waves and currents, the dynamic behavior of tidal inlet evolution have been studied through process-based numerical modelling (Wang et al., 1995; Marciano et al., 2005; Dissanayake, 2011; Dastgheib, 2012; Yu et al., 2012, 2014; Wang et al., 2014a, b).

Among the different aspects of the tidal inlet morphodynamics, the present study focuses on the problem of the incision of the main tidal channel. In decadal (~10^1 year or more) process-based models (van Maanen et al., 2016), the inlet development is often characterized by an unrealistic incision of the main tidal channel (Dissanayake, 2011; Dastgheib, 2012). In order to reduce the channel incision, several techniques have been adopted (van der Wegen, 2009): (1) increasing the effects of transverse bed slope transport to promote the stronger transverse downslope sediment transport; and (2) increasing the dry-cell erosion factor to stimulate bank erosion. In addition to the above methods, the effects including the spatial-temporal heterogeneous bedform roughness (Ganju and Sherwood, 2010) and bed sediment grain-size sorting (van der Wegen et al., 2011), are investigated in the present study.

The total bed roughness consists of bedform roughness, skin (grain) roughness, and

bed sediment motion roughness. The first part is the dominant component when bedforms develop (Smith and McLean, 1977; Xu and Wright, 1995). In the classification of van Rijn (2007a), with increasing dimensions, bedforms can be classified as ripples, mega-ripples, and dunes, which have typical roughness heights of 10^{-2} m, $10^{-2} \sim 10^{-1}$ m, and $10^{-1} \sim 10^{0}$ m, respectively. Bedform induced roughness is roughly proportional to sizes, especially the heights, and thus, dunes are the largest bedforms with the highest roughness. In tidal environments, because bedform size is related to grain size, water depth and flow velocity (Dalrymple et al., 1978; Ashley, 1990; Flemming, 2000; Bartholdy et al., 2002; Kubicki, A., 2008), the spatial-temporal heterogeneous sedimentologic and hydrodynamic environments result in the heterogeneities of bedform size and roughness. In deep tidal channels, due to coarse bed sediments, large water depth and strong current, large scale bedforms develop and dunes usually contribute as the major part of bedform roughness (Ernstsen et al., 2005; Buijsman and Ridderinkhof, 2008; Hughes et al., 2008; Barnard et al., 2013). For example, in the main tidal channel of the Marsdiep Inlet which is one of the inlets connecting Dutch Wadden Sea and the North Sea, observations show that dune heights range from 2 to 3 m. High dunes correspond to the deep trough of the channel, and the dune heights are larger than mega-ripple and ripple heights by at least an order of magnitude (Buijsman and Ridderinkhof, 2008). Bedform roughness heights can be estimated as a half of bedform heights (van Rijn, 2007a). Therefore, the bedform roughness heights reach up to 1.5 m and dominate the total bedform roughness, as well as the total roughness.

These large bedforms can pronouncedly increase the bed roughness, and then modify the sediment transport and morphological evolution (Tonnon et al., 2007). It is hypothesized that the elevated bed roughness is essential for the inlet channel development and is one of the key processes controlling the channel depth. The logic is that, the increases of water depth, bed sediment grain size, and current speed with respect to channel incision promote the bedforms (especially dunes) growth at the deep trough area, and the elevated bedform roughness enhances the flow drag and

then prevents the incision at the trough area.

The bedform roughness predictor (e.g., van Rijn (2007)) can calculate bedform (roughness) height in terms of current speed, bed sediment grain size and water depth. For tidal environments, the tidal variations of current speed may result in the tidal variations of bedform (roughness) heights. However, field evidence suggests that, compared with mega-ripples and ripples, the dune shape and height, can keep relatively stable during a tidal cycle (Allen, 1978; McCave and Langhorne, 1982; Harris and Collins, 1984, 1985; Gao et al., 1994; Salvatierra et al., 2015). For instance, the observations of dune dynamics in an inlet channel of the Danish Wadden Sea suggested that the dune heights varied from 2.1 to 2.4 m during a tidal cycle (Ernstsen et al., 2006). Meanwhile, dune dimensions respond to the hydrodynamic changes in a longer time span (i.e., changes in tidal averaged and peak velocity) but with pronounced lags and reduced rates (Langhorne, 1982; Flemming and Davis, 1992). Thus the dune roughness predictor should be modified to adjust to tidal environments. A relaxation option is implemented in some coastal hydrodynamic and morphodynamic modelling systems (e.g., Delft3D), but how to parameterize the "relaxation time scale" cannot be found in the previous literatures.

The pioneering work of Teske (2013) involved the bedform dynamics into decadal morphological modelling of the Amelander Inlet, which is another inlet of the Dutch Wadden Sea. Bedform roughness heights were simulated using van Rijn (2007a)'s method for hydrodynamic and sediment transport modelling. However, only the effects of ripples and mega ripples were taken into account in the models of Teske (2013). The field evidence in similar environments (water depth, bed sediments, tidal currents and waves) of the Marsdiep inlet suggests that, for the inlet tidal channels, the dune roughness is much larger than that of the mega-ripples and ripples (Buijsman and Ridderinkhof, 2008).

Another approach is involving sediment grain-size sorting processes. If multiple bed sediment fractions are employed in the morphodynamic model, their different transport capacities result in changes not only in the morphological evolution but also

the bed sediment composition (Geleynse, et al., 2011; Dissanayake and Wurpts, 2013). The strong currents within deep inlet channels cause bed coarsening which prevents channel incision (Dastgheib, 2012; Wang et al., 2014). Furthermore, bed sediment grain size variations also affect the bedform development (Ernstsen et al., 2005; van Rijn, 2007a), and thus, the sorting processes interact with the bedform development, which are possible to play a substantial role in channel morphodynamics.

The present study couples the bedform roughness and sediment grain-size sorting in the decadal morphodynamic modelling of the Amelander Inlet (Fig. 1), which is an inlet connecting the Dutch Wadden Sea and the south North Sea. Firstly, the contributions of different bedform types to the total bedform roughness and the usage of the van Rijn (2007a) bedform roughness predictor in tidal environments are investigated by short-term hydrodynamic modelling. Secondly, based on the tide only model as initial explorations, the effects of bedform roughness and sediment grain-size sorting were coupled in the morphodynamics in a decadal time scale. The objectives of the present study are to identify contributions of these two effects on the inlet channel morphodynamics, and find out the key factors controlling the channel incision.

2. Study Area

The Amelander Inlet is between the barrier islands of Terschelling and Ameland of the Dutch Wadden Sea (Fig. 1). It is the inlet with the least human interferences within the Dutch Wadden Sea and therefore shows the most natural behaviors. It is a typical meso-tidal inlet system with an ebb tidal delta, a main inlet channel, and a back-barrier tidal basin (Hayes, 1979). The basin area is about 270 km^2 and the tidal prism is ca. 480 million m^3 (Sha, 1989). The tidal forcing is characterized by a semidiurnal tide with a mean tidal range of 2.15 m, and the dominant wave direction is from northwest and the average significant wave height is about 1.0 m at the sea side of the inlet (Cheung et al., 2007). Within the inlet system, most of the bed

materials are fine sands with mean grain size of about 250 μm, and in the inlet channel area, the mean grain size increases to 300 - 400 μm. A key character of the main tidal channel of the Amelander Inlet is that, although the channel migrated periodically during the last 10^2 years, the maximum depth mostly keeps smaller than 25 m (Elias et al., 2012b; Teske, 2013).

3. Methods

3.1. Model description

Hydrodynamic modelling

In this study, a two-dimensional, depth-averaged (2DH) process-based morphodynamic model (Delft3D) was utilized (Lesser et al., 2004). The two-dimensional depth-averaged continuity equation and nonlinear, shallow-water momentum equations for incompressible free surface flow were solved numerically. In Delft3D-FLOW module, the computational part is protected against "dividing by zero" by assuming that the total water depth is at least 10% of the drying and flooding threshold (Dryflc). The threshold depth (SedThr) is defined as the minimum water depth for computing sediment transport.

Sediment transport and morphological evolution

Non-cohesive sediment transport was calculated by van Rijn (2007a, b)'s approach (see Delft3D-Flow manual for a full reference), and the standard advection-diffusion equation was employed for suspended sediment transport. Both suspended load and bed-load were involved in the Exner equation for sediment mass conservation to simulate the morphological changes. Due to the transverse bed slope, an additional bed-load transport vector perpendicular to the main bed-load transport vector is subsequently calculated with the parameter α_{bn} (Ikeda, 1982; van der Wegen, 2009). In order to save calculation time for long-term and medium-term modelling, the "online" approach suggested by Roelvink (2006) was adopted, which speeds up bed

adjustments by multiplying the bed sediment flux in each time step by a morphological scale factor (MF). This method has been successfully applied using a typical MF around 100 (Van der Wegen, 2009; Dissanayake, 2011; Dastgheib, 2012; Yu et al., 2012, 2014; Wang et al., 2014a, b).

Bedform roughness height prediction

For sandy bed (median bed sediment grain size D_{50} > 63 μm), the bedform roughness heights can be estimated using van Rijn (2007a)'s methods. It is noted that, in case of a simulation with multiple sediment fractions, the D_{50} of the grain mixture in the surface layer is used.

At first, the current mobility parameter ψ was defined as:

$$\psi = \frac{U_c^2}{(s-1)gD_{50}} \tag{1}$$

in which, s is the relative sediment density ($s = \rho_s / \rho_w$), and U_c is depth averaged current velocity.

The ripple roughness heights $k_{s,r}$ can be calculated as:

$$\begin{aligned} k_{s,r} &= \alpha_r \begin{cases} 150 f_{cs} D_{50} & \text{if } \psi \le 50 \\ (182.5 - 0.65\psi) f_{cs} D_{50} & \text{if } 50 < \psi \le 250 \\ 20 f_{cs} D_{50} & \text{if } \psi > 250 \end{cases} \\ f_{cs} &= \begin{cases} 1 & \text{if } D_{50} \le 0.25 D_{gravel} \\ (0.25 D_{gravel} / D_{50})^{1.5} & \text{if } D_{50} > 0.25 D_{gravel} \end{cases} \\ D_{gravel} &= 0.002 \text{ m} \end{aligned} \tag{2}$$

in which, α_r is the calibration factor for ripple roughness height prediction. The value of $k_{s,r}$ is limited to values ranging from D_{90} to 2% of the water depth.

The mega-ripple roughness heights $k_{s,mr}$ can be calculated as:

$$k_{s,mr} = \alpha_{mr} \begin{cases} 0.0002\, f_{fs} \psi h & \text{if } \psi \le 50 \\ (0.11 - 0.00002\psi)\, f_{cs} h & \text{if } 50 < \psi \le 550 \\ 0.02 & \text{if } \psi > 550 \end{cases}$$
$$f_{fs} = \begin{cases} D_{50} / 1.5 D_{sand} & \text{if } D_{50} < 1.5 D_{sand} \\ 1 & \text{if } D_{50} \ge 1.5 D_{sand} \end{cases} \quad (3)$$
$$D_{sand} = 0.000062 \text{ m}$$

in which, α_{mr} is the calibration factor for mega-ripple roughness height prediction, and h is the water depth. The value of $k_{s,mr}$ is limited to values smaller than 0.2 m.

The dune roughness heights $k_{s,d}$ can be calculated as:

$$k_{s,d} = \alpha_d \begin{cases} 0.0004\, f_{fs} \psi h & \text{if } \psi \le 100 \\ (0.048 - 0.00008\psi)\, f_{fs} h & \text{if } 100 < \psi \le 600 \\ 0 & \text{if } \psi > 600 \end{cases} \quad (4)$$

in which, α_d is the calibration factor for dune roughness height prediction, and the factor f_{fs} is the same as $k_{s,mr}$ prediction in eq. (3). Note that in this study $1.5 * D_{\text{sand}} < D_{50} < 0.25\, D_{\text{gravel}}$ thus $f_{\text{cs}} = f_{\text{fs}} = 1$.

In tidal environments, if the bedform volume is much larger the instantaneous (e.g., one hour sum) sediment transport rate, the bedform height (also its roughness height) lags behind the hydrodynamic variations within a tidal cycle and shows a relative constant value (Allen, 1978). In order to represent "the memory of old bedforms", a relaxation option was implemented for all three bedform roughness heights as given by:

$$\begin{aligned} k_{s,r} &= (1 - e^{-\Delta t / T_r}) k_{s,r,new} + e^{-\Delta t / T_r} k_{s,r,old} \\ k_{s,mr} &= (1 - e^{-\Delta t / T_{mr}}) k_{s,mr,new} + e^{-\Delta t / T_{mr}} k_{s,mr,old} \\ k_{s,d} &= (1 - e^{-\Delta t / T_d}) k_{s,d,new} + e^{-\Delta t / T_d} k_{s,d,old} \end{aligned} \quad (5)$$

where Δt is the time step of hydrodynamic updating, and T_r, T_{mr} and T_d are different relaxation time scales for the three bedform types. If the relaxation time scale T_* becomes zero, the corresponding relaxation factor $e^{-\Delta t / T^*}$ will be zero and the relaxation effect disappears.

The total bedform roughness height (k_s) predictor was given by:

$$k_s = \min(\sqrt{k_{s,r}^2 + k_{s,mr}^2 + k_{s,d}^2}, \frac{h}{2}) \quad (6)$$

The total bedform roughness height can be converted to the Chézy coefficient (C) and bed drag coefficient C_D for hydrodynamics modelling by:

$$C_D = g / C^2 = g / [18\log(\frac{12h}{k_s})]^2 \quad (7)$$

Sediment sorting with multi-fractions

In order to simulate the sediment sorting processes in the presence of multi-size sediment fractions, a multi-layer concept was applied (Deltares, 2014). The top-most layer is defined as the transport layer of constant thickness, a number of bookkeeping layers being included to track the bed stratigraphy. For the calculation of mixed-size sediment transport rate, the exposure and hiding effect on the non-cohesive sediment critical shear stress was estimated by the formulation of Wu et al. (2000) based on the transport layer sediment condition. Net deposited sediment is initially added to and mixed in the top-most layer until the defined constant thickness is exceeded. At that moment a new bookkeeping layer is created. When net erosion takes place, only sediments in the top-most layer are available to be picked up. Due to the different dynamics of mixed-size sediments, bed composition is adjusted with the sorting processes beginning in the top-most layer. The changes are then progressively transferred to the underlying layers. Every new bed surface grain-size composition influences the subsequent sorting process, which eventually results in the change of the total sediment transport rate and bed-level.

3.2. Model settings

Grid and bathymetry

The computational grid of the Amelander Inlet model is demonstrated as in Fig. 2a. The number of cells of flow grid is 169 and 163 in x and y direction, respectively. In the inlet area, the flow grid resolution is about 80 m by 100 m while in the offshore

area varies to about 800 m by 1400 m. Figure 2b shows the initial bathymetry of the whole model domain (data in meters relative to Dutch ordnance datum of the year 1999, from the Dutch ministry of public works) and focuses the thalweg, which is defined as the line of lowest elevation within a valley or watercourse. The locations of observation points O1 and O2 and cross-sections P1 - P4 within the focused thalweg area were marked in Fig. 2c.

Historical bathymetry data of the thalweg area in the years of 1975, 1989, 1999, 2011 were obtained from the Vaklodingen dataset, which was made available by the Dutch ministry of public works. This dataset covers the bathymetry of the Dutch coast, measured from 1928 up to present. With the measured data, historical changes of the tidal channel bathymetry can be investigated.

Tidal boundary conditions

Two types of flow boundaries were applied in the Amelander Inlet model. At the seaward edge of the domain harmonic water level boundary is applied and divided into 8 segments. Besides, the east and west boundaries are set to be Neumann, which prescribes the alongshore water level gradients over the length of lateral boundaries. In order to obtain the boundary conditions, the Amelander Inlet model was nested to the Dutch Wadden Sea model. Time series of water levels covering a spring-neap cycle at the Amelander Inlet model boundary were obtained from the Dutch Wadden Sea model, and the concept of "morphological tide" covering only a 24 hours 50 minutes period was employed to gives an optimal representation of the residual transports of a complete (neap-spring) tidal cycle (Latteux, 1995). The "morphological tide" on the boundary was derived by Jiao (2014) and then used for harmonic analysis. The resulted M2 and M4 tidal components were adopted as the tidal boundary of the present model.

Hydrodynamics and sediment dynamics

Both the drying and flooding threshold (Dryflc) and the threshold depth for computing sediment transport (SedThr) were set to 0.1 m. For the comparison of

different bed roughness settings, a uniform Chézy coefficient (58 $m^{0.5}s^{-1}$) in the whole domain or van Rijn (2007a)'s bed roughness predictor was applied in each run. To agree with the observed grain-size spectrum of surface sediments in the Amelander Inlet, two options of bed sediment were employed: one sand fraction of grain-size 250 μm, and two well mixed sand fractions comprising 150 μm (60%) and 400 μm (40%). The mean grain sizes D_m for both options are the same. The bed stratigraphy is composed of 120 layers, each 0.2 m thick, and the transport layer is defined to be 1 m thick, which is about a half of the bedform heights in the tidal channel (Parker, 1991). The morphological scale factor MF was set to 120 to speed up bed adjustments in terms of the previous similar longterm morphological modeling approaches (van der Wegen, 2009; Dastgheib, 2012; Yu et al., 2012, 2014). A simulation of one year morphological evolution with a smaller MF of 6 proved the applicability of the MF of 120 in the model. The relatively large transverse bedslope parameter for bedload α_{bn} of 25 (the default value is 1) was employed according to Van der Wegen (2009) and Teske (2013). α_{bn} is a sensitive parameter for channel incision, the high value for α_{bn} promoting the transverse downslope sediment transport to reduce the channel incision. All the other model parameters use default values in Delft3D (Deltares, 2014). Starting from measured bathymetry, the model simulated from 1999 to 2011, covering 12 years.

Case setups

Before the decadal morphodynamic modelling, short-term hydrodynamic tests were run to investigate (1) the influences of the dune relaxation time scale T_d on the tidal variations of dune roughness (T_d = 0 min, 745 min (i.e. one M2 tidal period), and 1490 min (i.e. two M2 tidal periods)) and (2) the relative importance of ripple, mega-ripple, and dune roughness heights at different locations. The former is to identify the proper values of T_d to keep the dune shape relatively stable during a tidal cycle, and the latter is to investigate the relative importance of the three types of bedforms. The model was run for 5 days from the initial bathymetry of 1999 and the bathymetry remained unchanged during the simulation.

Four cases were designed for the morphodynamic modelling, taking tidal forcing as the only driving force. The cases were categorized into two groups: case a1 and a2 used a uniform and constant Chézy coefficient of 58 $m^{0.5}s^{-1}$, and case b1 and b2 adopted the van Rijn (2007a)'s bed roughness predictor. When the bed roughness predictor was applied, the calibration factors α_r and α_{mr} for ripples and mega-ripples were set to the default values of 1.0, α_d for the most important dune roughness predictor is set to 2.0 to agree with the observations (see the results part). Because of the low variability of large scale bedforms and the high variability of small scale bedforms, the relaxation times of ripples and mega-ripples T_r, T_{mr} were simply set to 0 min, while the dune relaxation time T_d of 1490 min was used according to the short-term hydrodynamic tests above. The numbers "1" and "2" stand for a single sand fraction of 250 μm or two well mixed sand fractions of 150 μm (60%) and 400 μm (40%) at the initial state, respectively. The characterized settings are listed in Table 1.

4. Results

4.1. Historical bathymetry

Thalweg elevations were derived from measured bathymetry data of the thalweg area in the years of 1975, 1989, 1999, 2011 (Fig. 3). The profiles of thalweg elevations were projected on cross-section P4 (see the right panel). The historical bathymetries indicate that the channel depth is mostly not deeper than 26 m.

4.2. Short-term modelling results

The dune roughness height variations at the observation points in the channel (O2, for locations see Fig. 2c) were examined as an example, and the influences of dune relaxation time scale T_d can be distinguished from Fig. 4a. From the start time of the short-term modelling, the dune roughness heights series experienced two stages: firstly, $k_{s,d}$ was developing; and then, $k_{s,d}$ kept relatively stable and periodically changed according to tidal variations. The durations of the developing stages extended

following the increase of T_d: 0, 745, and 1490 min of T_d are associated with the duration of < 1/2 M2 period, ~ 1 M2 period, and ~ 1.5 M2 period, respectively. During the stage of stable dune roughness, as T_d increased, the strong tidal variations of dune roughness height $k_{s,d}$ vanishes: 0, 745, and 1490 min of T_d are in relation to tidal variations of $k_{s,d}$ from 0 to 1.21 m, 0.57 to 0.93 m, and 0.67 to 0.86 m, respectively. The tidal variation for $k_{s,d}$ with 1490 min of T_d is 26%, which is close to the observations in similar environments like an inlet channel of the Danish Wadden Sea (Ernstsen et al., 2006). Thus, large values of T_d can make $k_{s,d}$ respond to hydrodynamic changes (e.g. increase or decrease in tidal averaged and peak velocities over a long time span), but with reduced rates, as well as smooth the tidal variations of $k_{s,d}$. Both of these characteristics agree with the actual situations. Therefore, T_d of 1490 min was adopted for the decadal modelling.

At observation points O1 and O2 (for locations see Fig. 2c), the components of roughness heights for the short-term hydrodynamic tests with $T_r = T_{mr} = 0$ min and T_d = 1490 min were compared in Fig. 4b and Fig. 4c, respectively. O1 is at the lower part of intertidal area with mean depth of 0.8 m, where the predicted roughness heights of ripples, mega-ripples, and dunes have similar tidal variations ranging from 0 to 3 cm, and the ripple roughness is slightly larger than the others. Compared with the grain roughness of 2.5 times of D_{50}, the bed friction is dominated by the bedform effects. However, for the observation point in the channel with mean depth of 14.5 m (O2), the dune roughness height is overwhelmingly larger than the other components. The typical roughness heights of dune, mega-ripple, and ripples are 0.8, 0.1, and 0.03 m, respectively. According to eq. (6), for the observation point, the total bedform roughness height is roughly equal to the dune roughness height, indicating that the channel bed roughness is dominated by the development of dunes.

4.3. Decadal modelling results

The modelled bed elevation maps of the four cases in 2011 (12 years after 1999) of the whole domain and the thalweg area are shown in Fig. 5 and Fig. 6b-e, respectively. The thalweg positions are marked as the red curves (Fig. 6a-e), and the profiles of

modelled thalweg elevations are projected on cross-section P4 (Fig. 6f). The differences of channel incision between these cases are hard to distinguish from the maps. However, the thalweg elevations of these cases varies from each other: the maximum depth in 2011 is about 31 m, 26 m, 30 m and 25 m in case a1, a2, b1 and b2, respectively. It is worth noticing that only the final states of the 12th year's bed elevations are illustrated here, and the processes and trends of bed level evolution will be shown later to evaluate the performance of each case.

The present study focuses on the problem of unrealistic modelled channel incision, and thus the model performance were evaluated by the incision limits. The modelled thalwegs (Fig. 6f) all deviate from the observation of 2011 (Fig.3) to some extent, especially the thalweg positions. Not only the incision limits, but also the positions and other morphological characters are important for a comprehensive prediction skill. However, our first step is to find out the key factors controlling channel incision.

Mean sediment grain size D_m and combined roughness height after 12 years are obtained in the whole model domain, as well as in the thalweg area (Fig. 7). Sediments become coarser from initially 250 μm to above 350 μm in the channel, and finer to around 200 μm on the flats bordering the channel. This is in accordance with the observed data from the Geological Survey of the Netherlands (data source: www.tno.nl). The difference from case a2 and b2 are not obvious, regardless of using the method of Chézy or bed roughness predictor (Fig. 7a, b, e, f). Within the inlet channel, combined bed roughness height (k_s) reaches up to 1.0 - 1.5 m when using the bed roughness predictor, while it quickly decreases to < 0.25 m outside the channel (Fig. 7c, d, g, h). The channel k_s values of 1.0 - 1.5 m correspond to the dune heights of 2 - 3 m, which agree with the observations in the main tidal channel of the Marsdiep inlet, which is also in the Dutch Wadden Sea and has similar hydrodynamic and sedimentary environments (Buijsman and Ridderinkhof, 2008). Thus, the present model results of bed roughness are reliable with α_d = 2.0, although the field data of bedform dimensions are lacking for a direct comparison. Besides, case b2 shows larger area of high k_s than case b1 in the channel (Fig. 7g, h), indicating that coupling

sediment sorting with the bed roughness predictor will further reduce the channel incision and thus enhance the channel stability.

The evolution processes of bed elevation at different cross-sections have different patterns: P1 in most cases becomes shallower except in case b1, while P2 and P3 keep deepening throughout the 12 years (Fig. 8). Comparing the results at P2 and P3 of the four cases, it is found that in case a1 the channel deepening is the quickest and most intensive, case a2 and case b1 have almost the same rate of incision and thalweg depth, and in case b2 the incision is the mildest at quite reduced rates. This characteristics can be more clearly illustrated in Fig. 9: at P2 and P3, the thalweg elevation reduces the most sharply in case a1, while have similar incision rates in cases a2 and b1, and becomes deeper in the slowest rates in case b2 from the year of 1999 to 2011. For P1, both the cross-section profile (Fig. 8) and thalweg elevation (Fig. 9) show that only case b1 is associated with erosion but with reduced rate (~2m in 12 years). Thus, based on the incision trends at P1, P2, and P3, it is forecasted that in the near future, P2 and P3 would be deeper than P1 in case b1.

The impacts of bed roughness settings and grain size sorting are further investigated by comparing the modelled bed elevation, mean sediment grain size and bed drag coefficient C_D along cross-sections P1, P2 and P3 after 12 years (Fig. 10). The final bed levels along P2 and P3 show the largest incision in case a1, and the channel deepening in case a2 or b1 is close to each other, while the erosion is the smallest in case b2 (Fig. 10b, c). Bed sediments grow coarser in the deep channel with mean grain size of around 375 μm when introducing sediment sorting into the model, and the differences of the peak bed sediment grain size between using Chézy and roughness predictor method are limited (Fig. 10d - f). Meanwhile, larger bed drag coefficients induced by bedform roughness (i.e. larger bed frictions) are always associated with the channel area (Fig. 10g - h). Moreover, case b2 using two sediment fractions obtained slightly larger bed drag coefficients in the channel than case b1 of a single fraction, implying that in cases of bed roughness predictor, sediment grain-size sorting will induce larger bottom frictions in the channel.

5. Discussion

5.1. The effects of bedform roughness on tidal channel incision

The involvement of bedform roughness in the long-term morphological modeling can reduce tidal channel incision, which is attributed to two effects: (1) velocity for the whole tidal channel area decreases, and, (2) cross channel velocity distribution is modified, so that the velocity reduction in the deep area of the channel is larger than that in the shallow area.

The short-term hydrodynamic modelling results at the initial state in case a1 and b1 are shown in Fig. 11. Case b1 based on bedform roughness predictor corresponds to larger bed drag coefficient and, consequently, a reduction of tidal averaged current speed for the whole cross channel profile. The bed friction effects on the inlet current speed can be interpreted by the classic linear solution of current velocity in the inlet (Escoffier, 1940; de Swart and Zimmerman, 2009), indicating that the decrease of speed is proportional to the increase of bed drag coefficient at the inlet area.

Based on the bedform roughness predictor (eq. (1) - (7)) and assuming dune roughness is the major part of the total roughness, the ratio of roughness to water depth is proportional to the current mobility parameter ψ or the square of speed (eq.(1)), providing the speed is less than a critical value (e.g., 0.64 m/s and 0.78 m/s for D_{50} of 250 μm, 375 μm, respectively). Based on the White-Colebrook formulation (eq.(7)), the bed drag coefficient is proportional to the ratio of roughness to water depth. Thus, the area associated with higher current speed is corresponding to larger bed drag coefficient.

For the tidal inlet system, current speed in the inlet channel is higher than that in its seaward and landward shallow area, suggesting that when using the bedform roughness predictor, increase of bed drag coefficient and decrease of current speed in the channel area are both larger than that in the seaward and landward shallow area.

Sediment transport capacity is determined by the skin friction τ_s, which can be estimated by van Rijn (2007a, b):

$$\tau_s = gU^2 / [18\log_{10}(12h/1.5D_{50})]^2 \quad (8)$$

Because the channel area has more speed reduction than the seaward and landward shallow area, the decrease of sediment transport capacity is more pronounced. Thus, sediment transport gradients and the incision of inlet channel can thus be reduced.

Figure 11 also shows another effect of the bed roughness predictor on the channel current speed. The cross channel speed distribution is modified, so that the velocity reduction at deep area of the channel is larger than in the shallow area. For tidal inlet with sandy bed, bedforms, especially sand dunes, develop and dominate the bed friction on tidal flow. If the dune roughness is only proportional to the water depth, based on the relationship between C_D and k_s, the bed drag coefficient is a constant, which has the same effects as the definition of a constant Chézy coefficient. However, based on the bedform roughness predictor, the dune roughness is also proportional to the square of current velocity, implying that the deep channel area with high velocity is associated with large dunes and large bed drag coefficients. Thus, the application of dune roughness predictor can decrease the current velocity at the deep area in the channel (Fig. 11), resulting in reduced channel incision.

5.2. The effects of bed sediment sorting on tidal channel incision

The feedbacks of sediment gain-size sorting processes on morphological evolution have been pointed out in many coastal environments, including the tidal inlet system (Flemming et al., 1992; Nyandwi and Flemming, 1995; van der Wegen et al., 2011; Wang et al., 2014b). Strong tidal currents converge to inlet channels, resulting in bed erosion. Because of the mixing nature of bed sands, the sorting processes are more capable of removing fine grains than coarse sediments. The bed sediment mixture is consequently coarsened until approaching dynamic equilibrium, and then the bed sediment composition becomes stable. This process occurs, so that the mean bed sediment grain size at the observation point O2 (initial depth of 14.5 m) increases.

The initial value of mean bed sediment size is 250 μm, which approximately equals to the mean grain size of the whole study area, so it is also applied in the single sediment fraction cases a1 and b1. In case a2 and b2 with multiple fractions, the mean bed sediment size at O2 enhances from 250 μm to around 350 μm within the first 2 years, and then keeps relatively stable during the following 10 years (Fig. 12a). Compared with the evolution process of bed elevation (see Fig. 8, 9), the rate of change or the equilibrium time scale of bed sediment grain size is much faster or shortened than the morphological change, respectively. This has also been suggested by Wang et al. (2014a, b) for the tidal basin environment.

The sorted coarse bed sediments have significant influences on sediment transport, and consequently, on morphological change. According to the threshold velocity of sand motion formula (Miller et al., 1977) and bedload formula (Wang et al., 2001), with the same current velocity of 0.8 m/s at 1 m above the bed, the bedload transport rate for sediments of 375 μm is 0.7 times that of 250 μm grains. Moreover, based on Soulsby (1997), the sediment settling velocity for sediment grains of 375 μm is 1.6 times that of 250 μm, resulting in smaller Rouse number and reduced suspension. Thus, the coarser bed sediments within the channel area associated with grain-size sorting processes reduce the sediment transport rate pronouncedly, and therefore substantially prevent the channel incision.

The coupled effects of bedform roughness and sediment sorting on channel incision are not simply linear. According to eq. (1) to (4), bedform roughness is also related to the bed sediment grain size. D_{50} affects ψ, and thus the dune roughness, which is the major part of bed roughness in inlet channels, will also respond to sediment grain size sorting. Based on eq. (4) with α_d = 2.0, the relations between current speed and the bed roughness (represented by drag coefficient) for various sediment sizes are obtained. The two bed sediment conditions (D_{50} = 250, 375) have different patterns (Fig. 12b). For fine sediments of 250 μm, the drag coefficient rapidly increases with current speed until reaching the maximum value of 0.049 at a critical speed of 0.64 m/s, and decreases with increasing current speed thereafter. When sediments become

coarser, the maximum drag coefficient keeps the same, but the critical current speed increases to 0.78 m/s for D_{50} of 375 μm, and for large speed (> 0.75 m/s), the coarser sediment with D_{50} of 375 μm is associated with larger bed roughness (Fig. 12b). When the bed roughness predictor is applied, the typical current speed in the inlet channel is close to 0.8 m/s (tidally rms) (Fig. 11) or around 1 m/s (tidally peak). When sediment sorting process is involved, the typical channel bed sediment mean grain size increases from 250 to ~375 μm (Figs. 10, 12a). Therefore, when coupling both roughness predictor and sediment sorting, the > 0.75 m/s current speed and 375 μm sediment will cause the larger dune roughness, which may further prevent the channel incision (Fig. 12b). These increases of bedform dimensions (and also bed roughness) induced by grain-size coarsening have been proved by the field observations in the tidal inlets of the Danish Wadden Sea (Bartholdy et al., 2002; Ernstsen et al., 2005).

A possible argument may arise that sediment sorting seems to play more part on channel incision than bedform roughness in the 12-year modeling (Fig. 6). Explanations are proposed that the combined effects of grain-size sorting and bedform development resulted in the best modeling performances in case b2.The use of bedform roughness predictor also triggered the bedform (dunes) development stimulated by sediment sorting.

5.3. Calibration parameters α_d and T_d

Two important parameters, α_d and T_d, were used in the bedform (dune) roughness predictor (eq. (4)), with roughly calibrated values of 2 and 1490 min, respectively. The former was used to modify the predicted $k_{s,d}$ to fit the observations, and the latter was for smoothing the tidal variations of $k_{s,d}$.

In addition to the direct calibration with stable current velocity condition, the values of α_d are related to the tidal variations of current velocities. If the tidal current velocity can be expressed as a cosine function with tidal amplitude a, based on eqs. (1) and (4), provided $\psi < 100$ (e.g., for D_{50} of 375 μm, velocity amplitude below 0.78 m/s), the tidal averaged $k_{s,d}$ is proportional to $a^2/2$, while the peak $k_{s,d}$ is proportional to a^2.

According to Zarillo (1982), the dune is in equilibrium with peak tidal flow, and its dimensions remain stable within the tidal cycle, suggesting that the real tidal averaged $k_{s,d}$ should be proportional to a^2. Thus, a calibrated factor α_d of 2 is required for properly predicting $k_{s,d}$, and using α_d of 2 is suggested to be universal for tidal environments under the condition of ψ < 100. However, the typical current peak velocity in tidal inlet channel is around 1 m/s, which corresponds to the ψ of ~165 for D_{50} of 375 μm. The tidal responses of $k_{s,d}$ is more complicated (see Fig. 4a, $T_d = 0$), numerical results suggesting the ratio between the peak speed related $k_{s,d}$ and the tidal averaged $k_{s,d}$ is 1.43. Thus, the factor α_d induced by tidal effects should be between 1 and 2, depending on the peak current speed. The present calibrated values of 2 should be the combination of the tidal effects and the direct calibration of the predicting equation.

The values of T_d are related to the bed sediment transport rate, which is controlled by local bed sediment grain size and intensity of current velocity. The logic is that, intensive bed sediment transport causes quick dune dimension adjustment and pronounced dune height variations within a tidal cycle, which is associated with a small T_d. The observations of Ernstsen et al. (2006) show the tidal variations of dune heights from 2.1 to 2.4 m for 0.3 - 0.7 mm size of bed sands and 1.1 ms^{-1} peak depth-averaged tidal current velocity, while the dune heights vary from 1.1 to 2.2 m within a tidal cycle for 0.3 mm size of bed sands and 2.0 ms^{-1} peak depth-averaged tidal current velocity in the observations from Kostaschuk and Best (2005). The larger tidal variations of dune heights (smaller T_d) in the latter case could be explained by stronger tidal flow and finer bed sediment. Therefore, T_d is suggested to be site specific.

5.4. Future development of the model

The present study is only a tentative work on the combined effects of bedform roughness and sediment sorting on decadal morphodynamics. In addition to the van Rijn (2007a) bedform roughness predictor, which was employed in this study, other methods have to be involved in the model as more options, including (1) predicting

the bedform geometry (e.g., Allen, 1968; Nielsen, 1992; Yalin, 1992; Li et al., 1996, 1998; Yang et al., 2005; Van Landeghem et al., 2009); and (2) transferring bedform geometry to bedform roughness (e.g., Nielsen, 1992; Yalin, 1992; Li et al., 1996, 1998; Yang et al., 2005; Bartholdy et al., 2010).

Due to lack of the in-situ observations within the study area, the modelled bedform dimensions and dynamics are only compared with the field evidences in other similar tidal channels in the Wadden Sea area. In addition, the detailed hydrodynamic observations in the study area is important to reveal the performances of bedform roughness predictor on the hydrodynamic modelling. Thus, direct field observations is suggested for model calibration.

Although coupling bedform roughness predictor and sediment sorting in decadal morphodynamic modelling can significantly reduce the unrealistic inlet channel incision, several other processes, which are not included in the present model, may have the potential to influence morphological evolution. Waves not only modify the current flow field (Elias et al., 2012a; Orescanin et al., 2014; Wargula et al., 2014), but also transport sediments to the inlet mouth by longshore drift. Consequently, waves affect the channel incision (Bruun, 1978; Gao and Collins, 1994).

Another potential improvement is to add the anisotropy of the bedform roughness predictor. The predictor used in the present model based on eq. (1) to (4) does not distinguish the roughness in difference directions. For two-dimensional bedforms, which wildly appear in tidal inlets, their crest and trough lines are perpendicular to the main flow direction. The bedform roughness plays much more parts in resisting flow in the main flow direction than in any other directions, especially the direction of crest and trough lines. Thus, for non-unidirectional flow conditions, which are common in tidal environments, the anisotropic nature of bedform roughness is suggested to be taken into account in the future.

In addition, according the classic bedform phase diagram (Ashley, 1990), a certain type of bed sediment and current velocity is associated with only one type of

bedforms. For example, fine sandy bed and relatively low current velocities only lead to development of ripples, and mega-ripples or dunes cannot exist. Thus, in next generations of bedform roughness predictors, this kind of distinction should be implemented.

6. Conclusions

In the sandy tidal inlet system, bed roughness is dominated by bedform roughness, and within tidal channels, bedform roughness is dominated by dune roughness. The bedform roughness height predictor is a useful tool for determining spatial and temporal heterogeneous bed frictions in 2DH hydrodynamic modelling. A large relaxation time (2 M2 tidal periods) can smooth the tidal variations of dune roughness, and make it respond to hydrodynamic changes in a longer time scale. These characters of model results are consistent with the observations.

The performances of modelling the decadal inlet channel evolution can be considerably improved by introducing either bedform (dune) roughness predictor or sediment sorting processes. The mechanisms are twofold. First, in the deep channels where flow velocities are high, large dunes develop and cause large bed drag coefficients. When the bed roughness predictor is used, the incision reduces because the current speed in the inlet channel reduces, and the cross-sectional velocity distribution in the inlet is more homogeneous. Second, coarser bed sediments within the channel area induced by sorting prevent the channel incision. If both effects are coupled in the morphodynamic model, the inlet channel incision is further controlled, which is not just a result of the linear superposition of both effects, because sorting can further promote the development of dunes within the deep channels.

Acknowledgements

This study was supported by the National Key Basic Research Project in China

(2013CB956502), the Natural Science Foundation of China (NSFC 41206070, 41306076), the China Postdoctoral Science Foundation (2013T60519), and the Dutch Coastal Management and Maintenance research program that is executed in collaboration between Deltares and Rijkswaterstaat. YW and QY are grateful to Prof. Burg Flemming's inspiration and great help on bedform study. Edwin Elias, Jebbe van der Werf and Qinghua Ye in Deltares are also acknowledged for their help to the models in many aspects. The anonymous reviewer is much appreciated for insightful comments and valuable suggestions.

References:

Allen, J.R.L., 1968. The nature and origin of bedform hierarchies. Sedimentology 10, 161–172.

Allen, J.R.L., 1978. Computational models for dune time-lag: calculations using stein's rule for dune height. Sedimentary Geology 20, 165–216.

Anthony, A., J. Atwood, P. August, C. Byron, S. Cobb, C. Foster, C. Fry, A. Gold, K. Hagos, L. Heffner, D. Q. Kellogg, K. Lellis-Dibble, J. J. Opaluch, C. Oviatt, A. Pfeiffer-Herbert, N. Rohr, L. Smith, T. Smythe, J. Swift, and N. Vinhateiro. 2009. Coastal lagoons and climate change: ecological and social ramifications in U.S. Atlantic and Gulf coast ecosystems. Ecology and Society 14(1), 8.

Ashley, G.M., 1990. Classification of large-scale subaqueous bedforms: a new look at an old problem. J. Sediment. Petrol. 60, 160–172.

Barnard, P., Erikson, L.H., Elias, E.P.L., Dartnell, P., 2013. Sediment transport patterns in the San Francisco Bay Coastal System from cross-validation of bedform asymmetry and modeled residual flux. Marine Geology 345, 72–95.

Bartholdy, J., Bartholomae, A., Flemming, B.W., 2002. Grain-size control of large compound flow-transverse bedforms in a tidal inlet of the Danish Wadden Sea. Marine Geology 188, 391–413.

Bartholdy, J., Flemming, B.W., Ernstsen, V.B., 2010. Hydraulic roughness over simple subaqueous dunes. Geo-Marine Letters 30, 63–76.

Bruun, P., 1978. Stability of Tidal Inlets. Elsevier, New York, 510 pp.

Buijsman, M.C., Ridderinkhof, H., 2008. Long-term evolution of sand waves in the Marsdiep inlet. I: high-resolution observations. Continental Shelf Research 28, 1202–1215.

Cheung, K.F., Gerritsen, F., Cleveringa, J., 2007. Morphodynamics and sand bypassing at ameland inlet, the Netherlands. Journal of Coastal Research 23, 106-118.

Dalrymple, R.W., Knight, R.J., Lambiase, J.J., 1978. Bedforms and their hydraulic stability relationships in a tidal environment, Bay of Fundy, Canada. Nature 275, 100–104.

Dastgheib, A., 2012. Long-term process-based morphological modelling of large tidal basins. Ph.D. Thesis, UNESCO-IHE, Delft, the Netherlands.

De Fockert, A., 2008. Impact of relative sea level rise on the Amelander inlet Morphology. Master thesis, Delft University, Delft, the Netherlands.

Deltares, 2014. User Manual Delft3D-FLOW, version: 3.15.34158. Deltares, Delft, the Netherlands, pp. 710.

de Swart, H.E., Zimmerman, J.T.F., 2009. Morphodynamics of Tidal Inlet Systems. Annual Review of Fluid Mechanics 41, 203–229.

Dissanayake, P., Wurpts, A., 2013. Modelling an anthropogenic effect of a tidal basin evolution applying tidal and wave boundary forcings: Ley Bay, East Frisian Wadden Sea. Coastal Engineering 82, 9–24.

Dissanayake, P.K., 2011. Modelling morphological response of large tidal inlet systems to sea level rise. Ph.D. Thesis, UNESCO-IHE, Delft.

Elias, E. P. L., Gelfenbaum, G., Van der Westhuysen, A. J., 2012a. Validation of a coupled wave-flow model in a high-energy setting: The mouth of the Columbia River. J. Geophys. Res. 117, C09011, doi:10.1029/2012JC008105.

Elias, E., van der Spek, A., Wang, Z., De Ronde, J., 2012b. Morphodynamic development and sediment budget of the Dutch Wadden sea over the last century. Netherlands Journal of Geosciences 91, 293–310.

Ernstsen, V.B., Noormets, R., Winter, C., Hebbeln, D., Bartholomae, A., Flemming, B.W., Bartholdy, J., 2005. Development of subaqueous barchanoid-shaped dunes due to lateral grain size variability in a tidal inlet channel of the Danish Wadden Sea. J. Geophys. Res. 110, F04S08, doi:10.1029/2004JF000180.

Ernstsen, V.B., Noormets, R., Winter, C., Hebbeln, D., Bartholomae, A., Flemming, B.W., Bartholdy, J., 2006. Quantification of dune dynamics during a tidal cycle in an inlet channel of the Danish Wadden Sea. Geo-Mar. Lett. 26, 151–163.

Escoffier, F. F., 1940. The stability of tidal inlets. Shore Beach 8, 114–115.

FitzGerald, D.M., Fenster, M.S., Argow, B.A., Buynevich, I.V., 2008. Coastal impacts due to sea-level rise. Annual Review of Earth and Planetary Sciences 36, 601–647.

Flemming, B.W., 2000. The role of grain size, water depth and flow velocity as

scaling factors controlling the size of subaqueous dunes. In: Trentesaux, A., Garlan, T. (Eds.), Marine SandWave Dynamics. InternationalWorkshop, Lille, France, pp. 55–60.

Flemming, B.W., Davis, R.A., 1992. Dimensional adjustment of subaqueous dunes in the course of a spring–neap semicycle in a mesotidal backbarrier channel environment (German Wadden Sea, southern North Sea). In: Flemming BW (ed) Tidal Clastics 92, Proc 3rd Int Res Symp Modern and Ancient Clastic Tidal Deposits. Senckenberg Institute, Wilhelmshaven, Germany, pp 28–30.

Flemming, B.W., Nyandwi, N., 1994. Land reclamation as a cause of fine-grained sediment depletion in backbarrier tidal flats (southern North Sea). Netherlands Journal of Aquatic Ecology 28, 299–307.

Flemming, B.W., Schubert, H., Hertweck, G., Müller, K., 1992. Bioclastic tidal-channel lag deposits: a genetic model. Senckenbergiana Maritima 22, 109–129.

Ganju, N.K., Sherwood, C.R., 2010. Effect of roughness formulation on the performance of a coupled wave, hydrodynamic, and sediment transport model. Ocean Modelling 33, 299–313.

Gao S., Collins M., Lanckneus J., De Moor, G., van Lancker V., 1994. Grain size trends associated with net sediment transport patterns, an example from the Belgian continental shelf. Marine Geology 121, 171-185.

Gao, S., Collins, M.B., 1994. Tidal inlet equilibrium in relation to cross-sectional area and sediment transport patterns. Estuarine, Coastal and Shelf Science 38, 157–172.

Geleynse, N., Storms, J.E.A., Walstra, D.-J.R., Jagers, H.R.A., Wang, Z.B., Stive, M.J.F., 2011. Controls on river delta formation; insights from numerical modelling. Earth and Planetary Science Letters 302, 217–226.

Hardisty, J., 1983. An assessment and calibration of formulations for Bagnold's bedload equation. Journal of Sedimentary Petrology 53, 1007– 1010.

Harris, P.T., Collins, M.B., 1984. Side-scan sonar investigation into temporal variation in sandwave morphology: Helwick Sands, Bristol Channel. Geo-Mar. Lett. 4, 91–97.

Harris, P.T., Collins, M.B., 1985. Bedford distributions and sediment transport paths in the Bristol Channel and Severn Estuary, U.K. Marine Geology 62, 153–166.

Hayes, M.O., 1979. Barrier island morphology as a function of tidal and wave regime. In: Leatherman, S.P. (Ed.), Barrier islands from the Gulf of St. Lawrence to the Gulf of Mexico. Academic Press, New York, 211-236.

Hughes, M.G., Harris P.T., Heap A., Hemer, M.A., 2008. Form drag is a major component of bed shear stress associated with tidal flow in the vicinity of an

isolated sand bank, Torres Strait, northern Australia. Continental Shelf Research 28, 2203– 2213.

Ikeda, S., 1982. Lateral bed load transport on side slopes, Journal Hydraulics Division, ASCE 108(11), 1369–1373.

IPCC, 2007. Climate change 2007: the physical science basis, summary for policymakers. Contribution of Working Group I to the Fourth Assessment Report of the Intergovernmental Panel on Climate Change, Cambridge, UK.

Jiao, J., 2014. Morphodynamics of Ameland Inlet: medium-term Delft3D modelling. Master thesis, Delft University, Delft, The Netherlands.

Kostaschuk, R., Best, J., 2005. Response of sand dunes to variations in tidal flow: Fraser Estuary, Canada, J. Geophys. Res. 110, F04S04, doi:10.1029/2004JF000176.

Kubicki, A., 2008. Large and very large subaqueous dunes on the continental shelf off southern Vietnam, South China Sea. Geo-Mar. Lett. 28, 229–238.

Langhorne, D.N., 1982. A study of the dynamics of a marine sandwave. Sedimentology 29, 571–594.

Latteux, B., 1995. Techniques for long-term morphological simulation under tidal action. Marine Geology 126, 129–141.

Lee, H.J., Chu, Y. S., Park, Y.A., 1999. Sedimentary processes of fine-grained material and the effect of seawall construction in the Daeho macrotidal flat–nearshore area, northern west coast of Korea. Marine Geology 157, 171–184.

Lesser, G.R., Roelvink, J.A., van Kester, J.A.T.M., Stelling, G.S., 2004. Development and validation of a three-dimensional morphological model. Coastal Eng. 51, 883–915.

Li, M.Z., Amos, C.L., 1998. Predicting ripple geometry and bed roughness under combined waves and currents in a continental shelf environment. Cont. Shelf Res. 18, 941–970.

Li, M.Z., Wright, L.D., Amos, C.L., 1996. Predicting ripple roughness and sand suspension under combined flows in a shoreface environment. Marine Geology 130, 139– 161.

Marciano, R., Wang, Z.B., Hibma, A., de Vriend, H.J., Defina, A.. 2005. Modeling of channel patterns in short tidal basins. Journal of Geophysical Research 110, F01001, doi: 10.1029/2003JF000092.

McCave, I.N., Langhorne, N., 1982. Sand waves and sediment transport around the end of a tidal sandbank. Sedimentology 29, 95–110.

Miller, M.C., McCave, I.N., Komar, P.D., 1977. Threshold of sediment motion under

unidirectional currents. Sedimentology 24, 507–527.

Nielsen, P., 1992. Coastal bottom boundary layers and sediment transport. Advanced Series on Ocean Engineering. World Scientific, Singapore.

Orescanin, M., Raubenheimer, B., Elgar, S., 2014. Observations of wave effects on inlet circulation, Continental Shelf Research 82, 37–42.

Parker G., 1991. Selective sorting and abrasion of river gravel, I: Theory. Journal of Hydraulic Engineering, 117, 131–149.

Reise, K., 2001. Ecological Comparison of Sedimentary Shores. Heidelberg, Berlin, Springer-Verlag, 384 pp.

Salvatierra, M.M., Aliotta, S., Ginsberg, S.S., 2015. Morphology and dynamics of large subtidal dunes in Bahia Blanca estuary, Argentina. Geomorphology 246, 168–177.

Sha, L., 1989. Variation in ebb-delta morphologies along the west and east Frisian islands, the Netherlands and Germany. Marine Geology 89, 11–28.

Smith J.D., McLean S.R., 1977. Spatially averaged flow over a wavy surface. Journal of Geophysical Research 82, 1735–1746.

Teske, R., 2013. Tidal inlet channel stability in long term process based modelling. MSc. traineeship report, Deltares, 78 pp.

Tonnon, P.K., van Rijn, L.C., Walstra, D.J.R., 2007. The morphodynamic modeling of tidal sand waves on the shoreface. Coastal Engineering 54, 279–296.

van der Wegen, M., 2009. Modeling morphodynamic evolution in alluvial estuaries. Ph.D. Thesis, UNESCO-IHE, Delft, the Netherlands.

van der Wegen, M., 2013. Numerical modeling of the impact of sea level rise on tidal basin morphodynamics. J. Geophys. Res. Earth Surf. 118, 447–460, doi:10.1002/jgrf.20034.

van der Wegen, M., Jaffe, B.E., Roelvink, J.A., 2011. Process-based, morphodynamic hindcast of decadal deposition patterns in San Pablo Bay, California, 1856–1887, J. Geophys. Res. 116, F02008, doi:10.1029/2009JF001614.

van Goor, M.A, Zitman, T.J., Wang, Z.B., Stive, M.J.F., 2003. Impact of rising sea level on the morphologic equilibrium state of tidal inlets. Marine Geology 202, 211–227.

Van Landeghem, K.J.J., Wheeler, A.J., Mitchell, N.C., Suttond, G., 2009. Variations in sediment wave dimensions across the tidally dominated Irish Sea, NW Europe. Marine Geology 263, 108–119.

van Maanen, B., Nicholls, R.J., French, J.R., Barkwith, A., Bonaldo, D., Burningham, H., Murray, A.B., Payo, A., Sutherland, J., Thornhill, G., Townend, I.H., van der Wegen, M., Walkden, M.J.A., 2016. Simulating mesoscale coastal evolution for

decadal coastal management: A new framework integrating multiple, complementary modelling approaches. Geomorphology 256, 68–80.

van Rijn, L.C., 2007a. Unified view of sediment transport by currents and waves I: Initiation of motion, bed roughness and bed-load transport. Journal of Hydraulic engineering 133, 649–667.

van Rijn, L.C., 2007b. Unified view of sediment transport by currents and waves II: Suspended Transport. Journal of Hydraulic engineering 133, 668–689.

Wang, Y.P., Gao, S., 2001. Modification to the Hardisty equation, regarding the relationship between sediment transport rate and particle size. Journal of Sedimentary Research 71, 118– 121.

Wang, Y.W., Yu, Q., Gao, S., 2014. Modeling interrelationships between morphological evolution and grain-size trends in back-barrier tidal basins of the East Frisian Wadden Sea. Geo-marine Letters 34, 37–49.

Wang, Y.W., Yu, Q., Gao, S., Flemming, B., 2014. Modeling the effect of progressive grain-size sorting on the scale dependence of back-barrier tidal basin morphology. Continental Shelf Research 91, 26–36.

Wang, Z.B., Hoekstra, P., Burchard, H., Ridderinkhof, H., De Swart, H.E., Stive, M.J.F., 2012. Morphodynamics of the Wadden Sea and its Barrier Island System. Ocean & Coastal Management 68, 39–57.

Wang, Z.B., Louters, T., de Vriend, H.J., 1995. Morphodynamic modeling of a tidal inlet in the Wadden Sea. Marine Geology 126, 289–300.

Wargula, A., Raubenheimer, B., Elgar, S., 2014. Wave-driven along channel subtidal flows in a well-mixed ocean inlet. J. Geophys. Res. Oceans 119, 2987–3001, doi: 10.1002/2014JC009839.

Wu W., Wang S.S.Y., Jia Y., 2000. Nonuniform sediment transport in alluvial rivers. Journal of Hydraulic Research 38(6), 427–434.

Xu, J.P., Wright, L.D., 1995. Tests of bed roughness models using field data from the Middle Atlantic Bight. Continental Shelf Research 15, 1409-1434.

Yalin, M.S., 1992. River mechanics. Exeter, Pargamon Press, 219pp.

Yang S.-Q., Tan S.-K., Lim S.-Y., 2005. Flow resistance and bed form geometry in a wide alluvial channel. Water Resources Res 41, W09419. doi: 10.1029/2005WR004211

Yu, Q., Wang, Y.W., Flemming, B. W., Gao, S., 2014. Scale-dependent characteristics of equilibrium morphology of tidal basins along the Dutch-German North Sea coast. Marine Geology 348, 63–72.

Yu, Q., Wang, Y.W., Flemming, B.W., Gao, S., 2012. Modelling the equilibrium hypsometry of back-barrier tidal flats in the German Wadden Sea (southern

North Sea). Continental Shelf Research 49, 90–99.

Zarillo, G.A., 1982. Stability of bedforms in a tidal environment. Marine Geology 48, 337–351.

Table1. Setups in the 4 cases

Case	Sediment fraction	Bed roughness setting
a1	1	C = 58
a2	2	C = 58
b1	1	VR07, α_r = 1, α_{mr} = 1, α_d = 2
b2	2	VR07, α_r = 1, α_{mr} = 1, α_d = 2

The numbers of 'Sediment fraction' denote a single sand fraction of 250 μm or two well mixed sand fractions of 150 μm (60%) and 400 μm (40%), respectively. 'C = 58' and 'VR07' represent using a constant Chézy coefficient of 58 $m^{0.5}s^{-1}$ and van Rijn (2007)'s bedform roughness height predictor, respectively. The values of the calibration factors are listed.

Figure captions

Fig. 1. the Amelander inlet (data from the Dutch ministry of public works)

Fig. 2. (a) Model grid; (b) Initial bathymetry of the model domain; (c) Initial bathymetry of the thalweg area (focused area in Fig. 2b) (O1 and O2: observation points; P1 - P4: cross-sections)

Fig. 3. Bathymetry in the thalweg area in 1975, 1989, 1999, 2011 (in meters relative to Dutch ordnance datum) and the thalweg elevations (x-axis increases southward along P4, data from the Dutch ministry of public works)

Fig. 4. Short-term hydrodynamic model results at observation point O1 and O2 (mean water depth is 0.8 m and 14.5 m, respectively) from the initial state of 1999: (a) Dune roughness height $k_{s,d}$ of O2 predicted by different dune relaxation time T_d from 0 to 50th hour after the start of model, indicating the development and stability of $k_{s,d}$; (b, c) Components of roughness heights of O1 and O2 ($T_r = T_{mr} = 0$ min, $T_d = 1490.0$ min) from 67th to 117th hour after model started, when all roughness heights remained stable

Fig. 5. Modelled bed elevation after 12 years: (a) case a1; (b) case a2; (c) case b1; (d) case b2.

Fig. 6. Modelled bed elevation after 12 years in the thalweg area: (a) the initial state, (b) case a1, (c) case a2, (d) case b1, (e) case b2; and the thalweg elevation (panel f, x-axis increases southward along P4).

Fig. 7. Modelled mean sediment grain size D_m and combined roughness height after 12 years in the whole model domain (a-d) and the thalweg area (e-h), respectively

Fig. 8. Bed elevation of cross-section P1, P2 and P3 at initial state, 3rd, 6th, 9th, 12th year, respectively

Fig. 9. Evolution processes of thalweg elevation of cross-section P1, P2 and P3 in the four cases

Fig. 10. Modelled bed elevation, mean sediment grain size and bed drag coefficient of cross-section P1, P2 and P3 after 12 years

Fig. 11. Bed elevation, Chézy coefficient and tidal-averaged rms current speed of cross-section P2 at the initial state in case a1 and b1, respectively

Fig. 12. (a) Evolution processes of mean grain size at O2 (initial water depth is 14.5 m) in case a2 and b2; (b) Relation between current speed and the bed drag coefficient (It is noted that, based on eqs. (4) and (7), the drag coefficient is independent with the water depth)

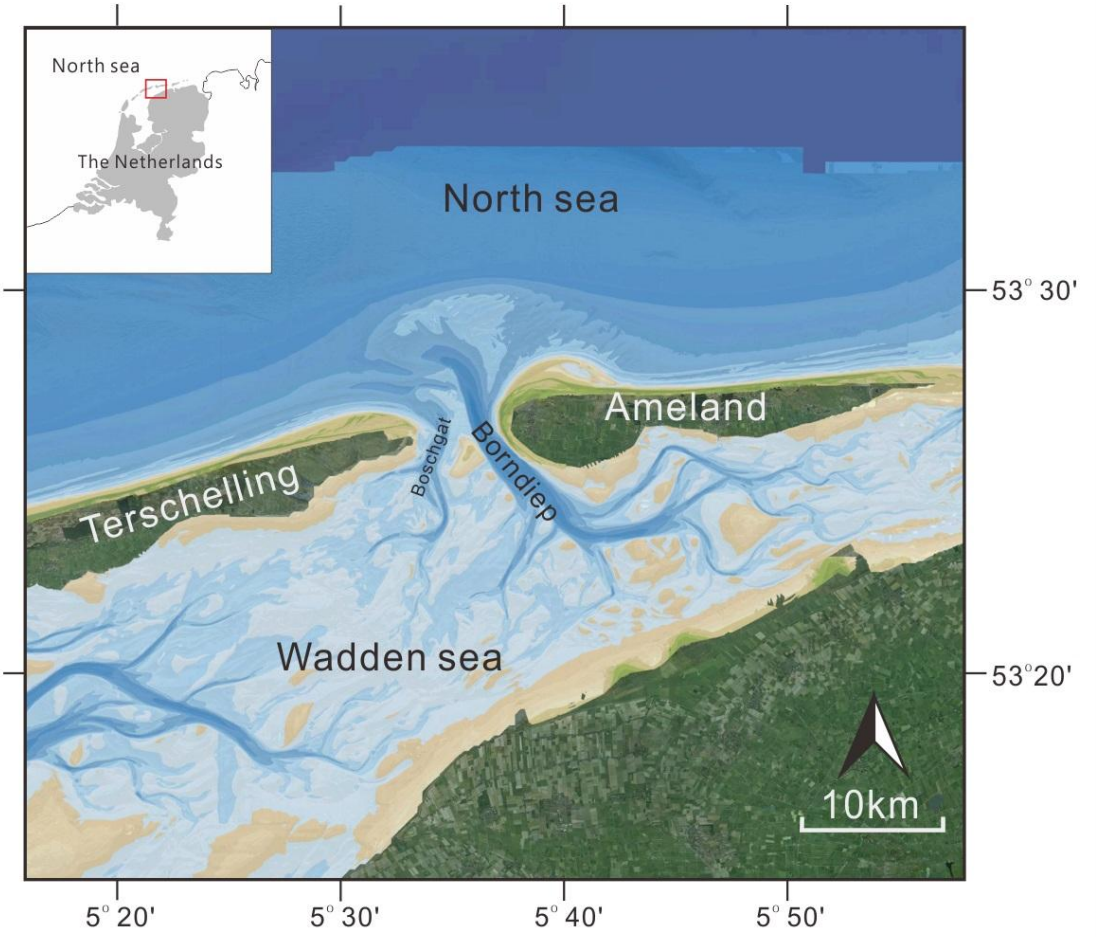

Figure 1

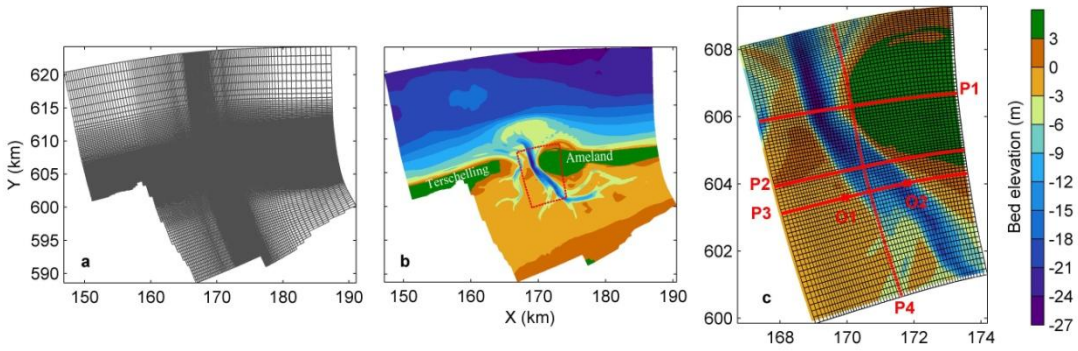

Figure 2

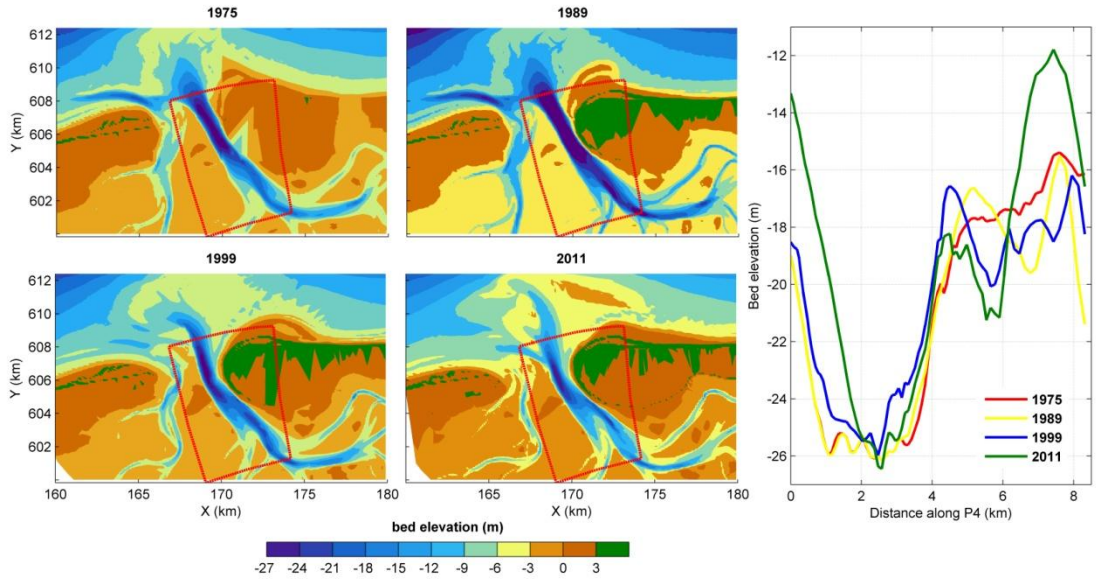

Figure 3

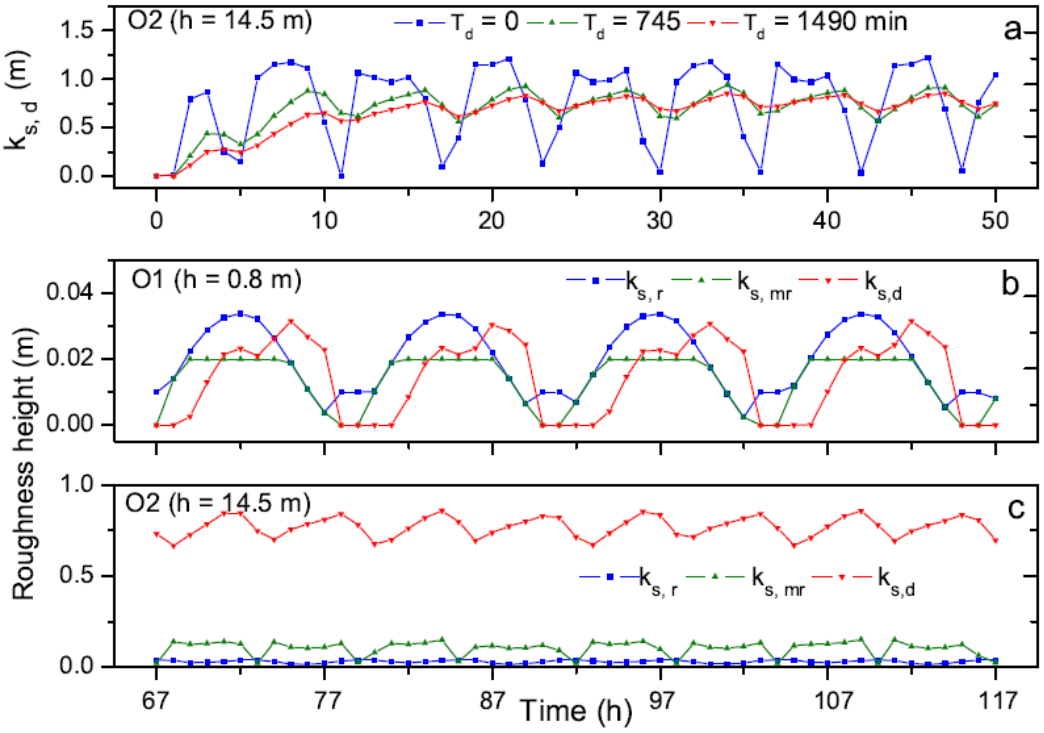

Figure 4

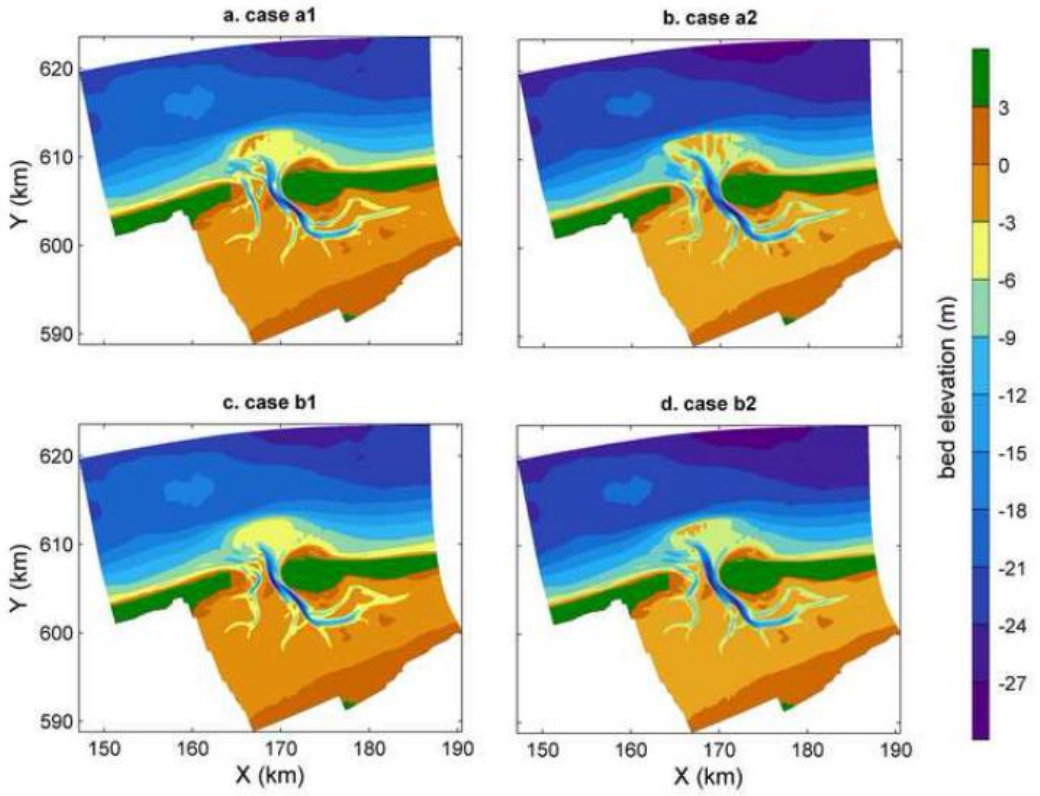

Figure 5

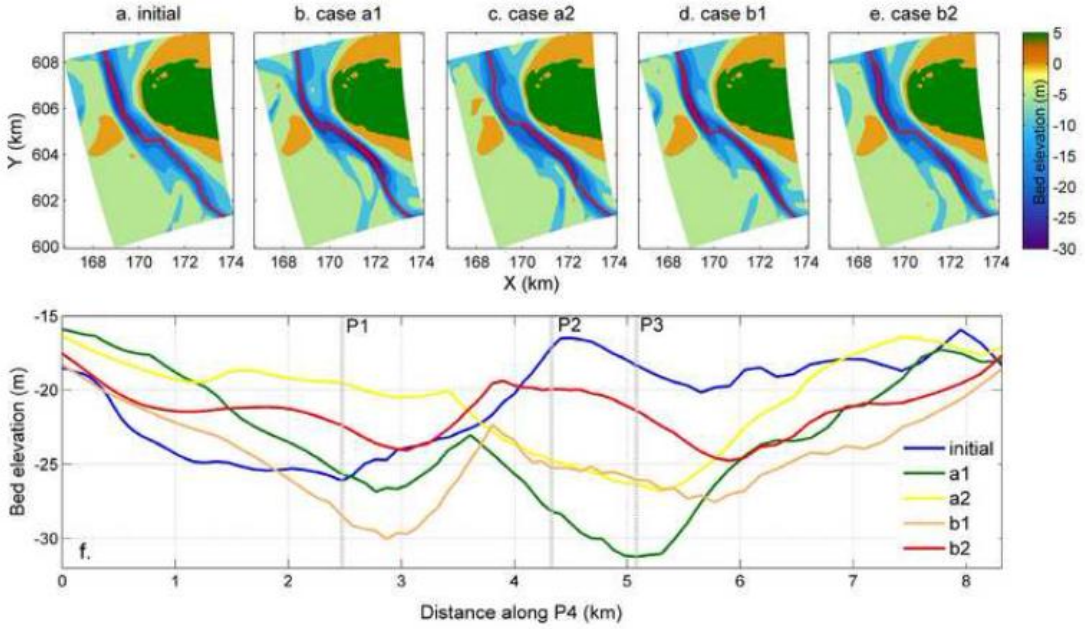

Figure 6

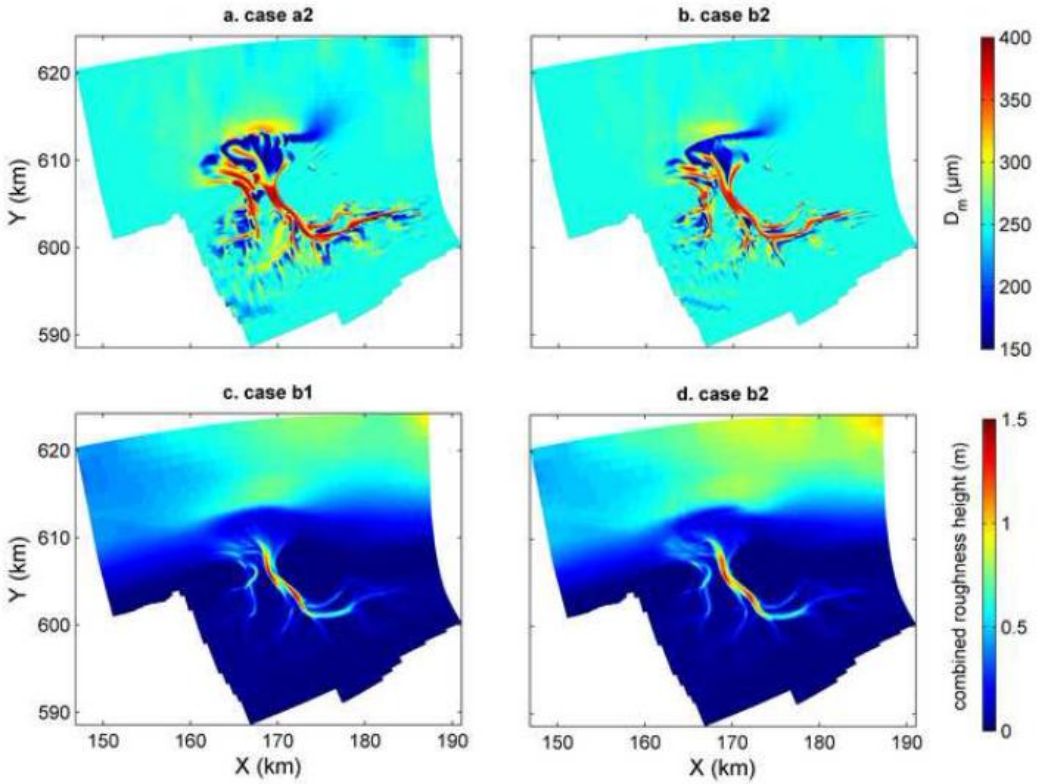

Figure 7a-d

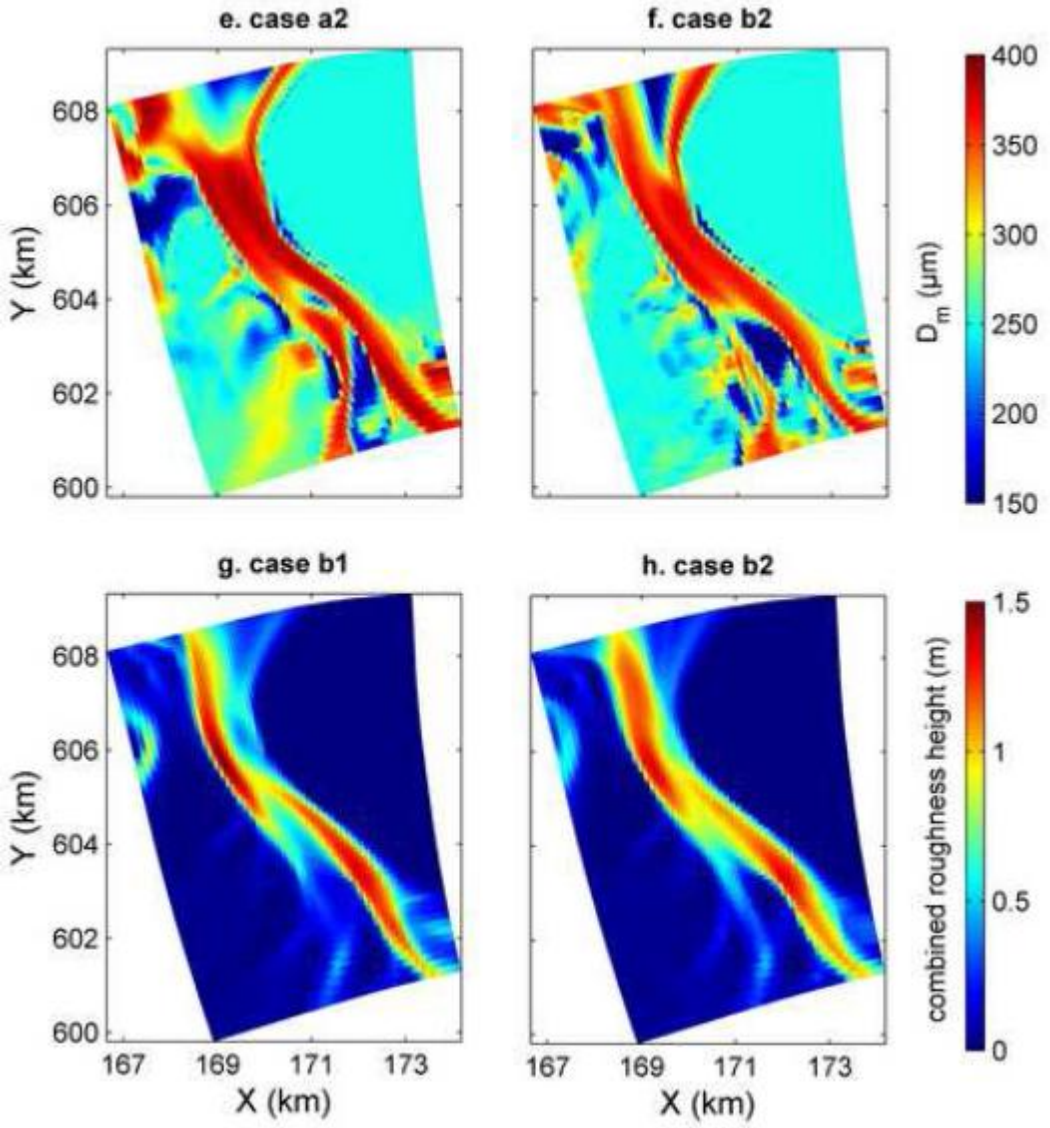

Figure 7e-h

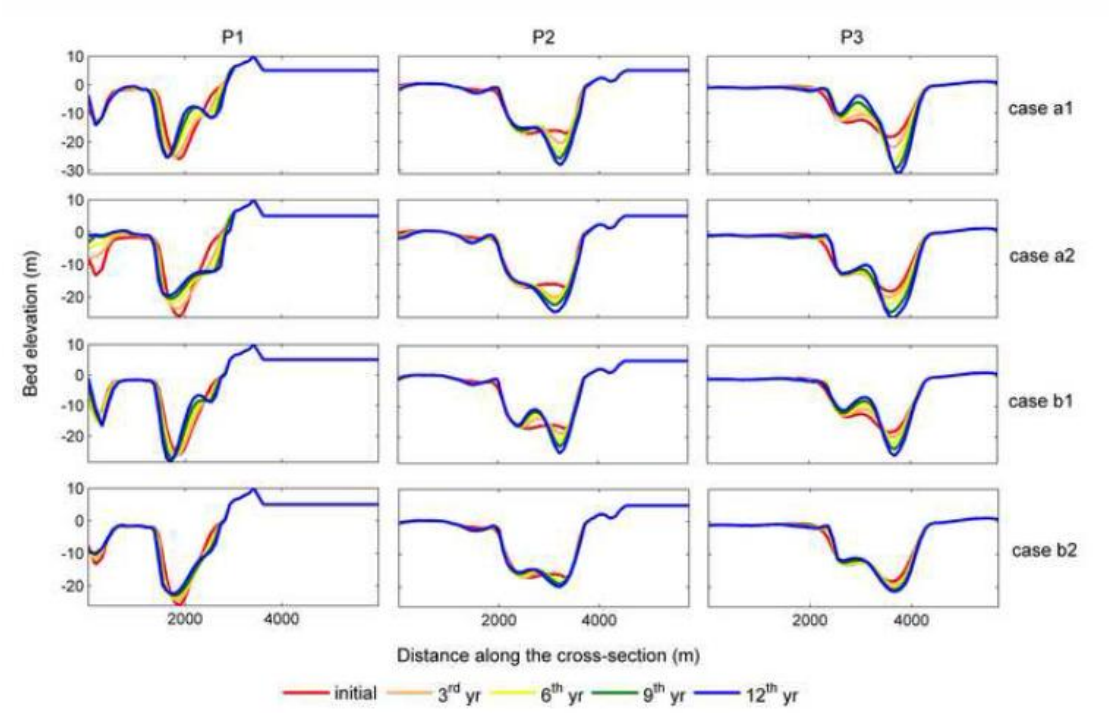

Figure 8

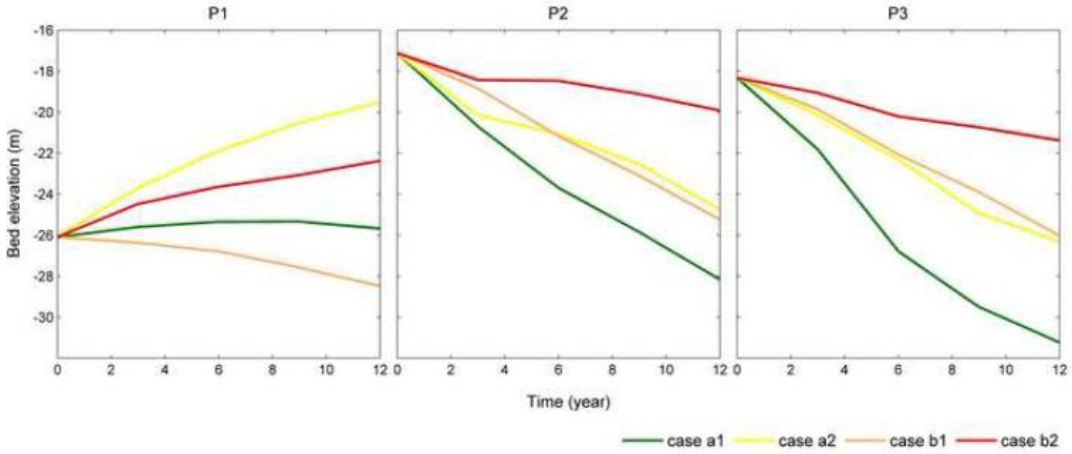

Figure 9

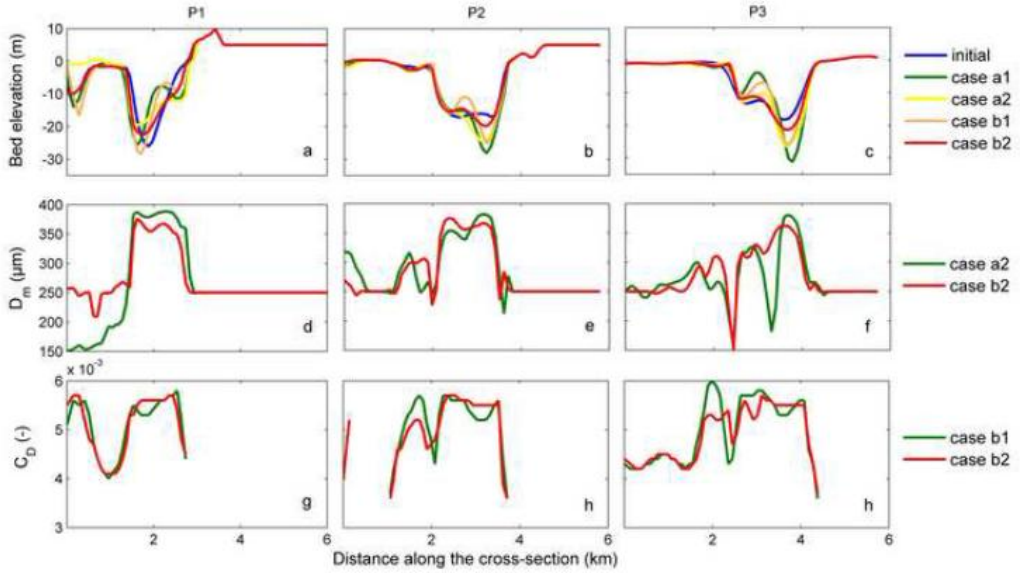

Figure 10

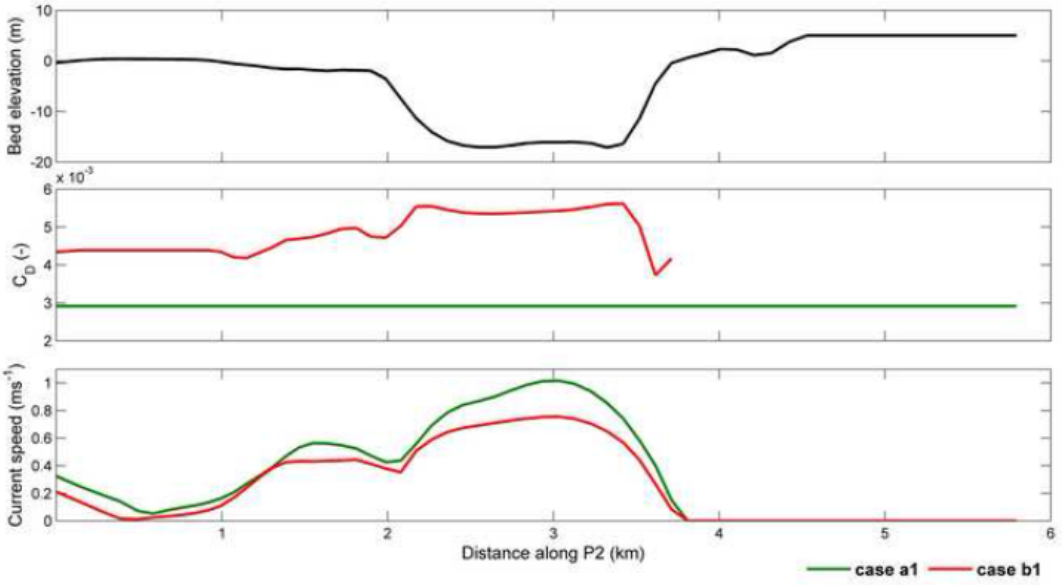

Figure 11

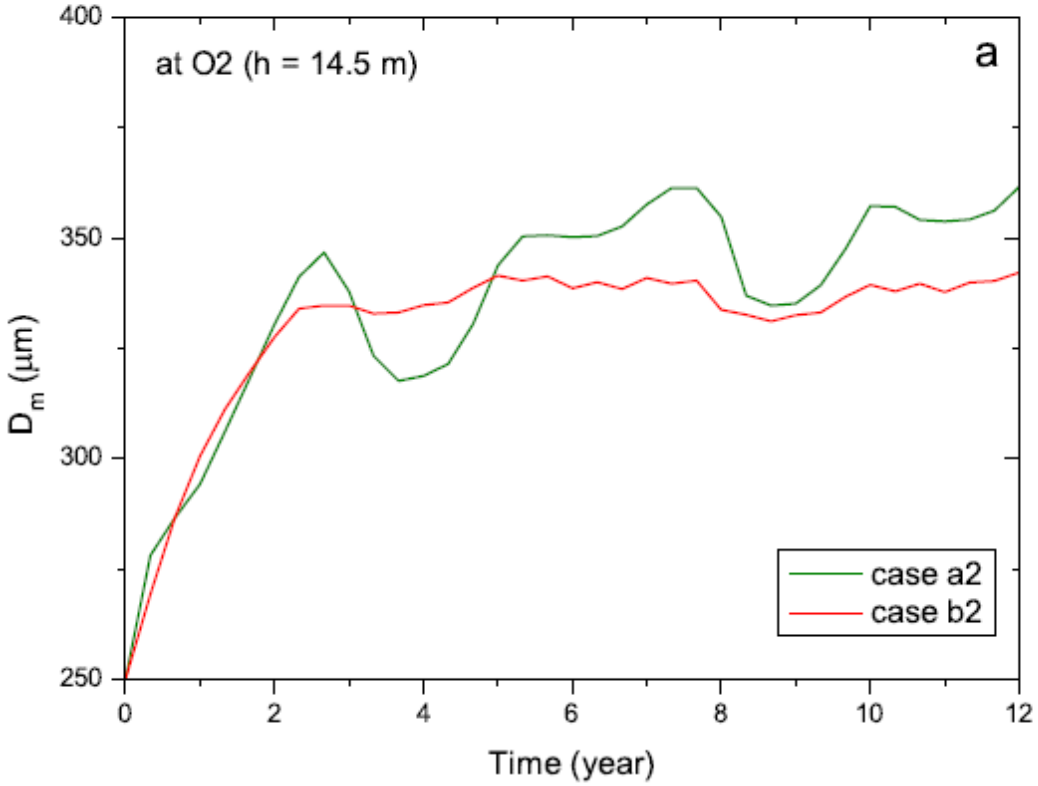

Figure 12a

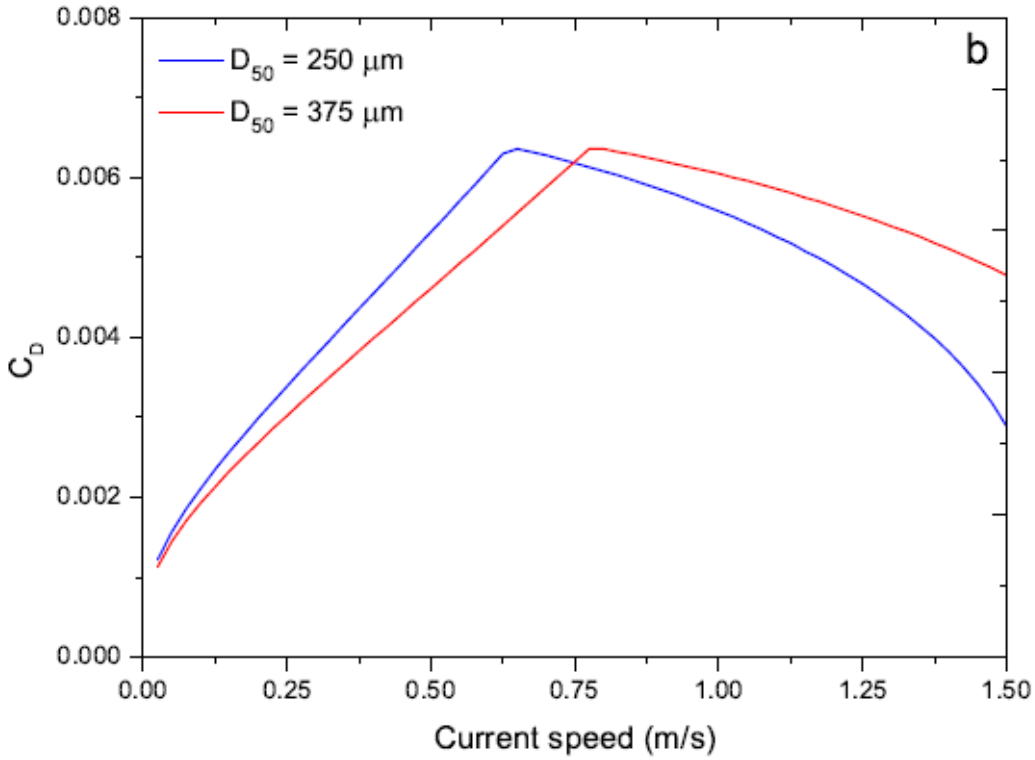

Figure 12b

Highlights:

- ✓ Bedform roughness height predictor is a useful tool for determining heterogeneous bed frictions
- ✓ Large dunes and coarser bed sediment in deep channels reduce incision
- ✓ Sediment sorting further promotes the development of dunes within the deep channels